2D metal-organic framework Cu₃(HHTP)₂ composite electrode for flexible energy storage applications

Maria Prince [a], Jithin Kanathedath [a], Febin Paul [a], Prasutha Rani Markapudi [a], Mustehsan Beg [a], Lynn Paterson [b], Marc PY. Desmulliez [b], Suresh C. Pillai [c], Libu Manjakkal [a],*

[a] School of Computing and Engineering & the Built Environment Edinburgh Napier University, Merchiston Campus, EH10 5DT, Edinburgh, UK
[b] School of Engineering and Physical Sciences, Heriot-Watt University, Edinburgh, UK
[c] Nanotechnology Research Group, Department of Environmental Science, Atlantic Technological University, ATU Sligo, Ash Lane, Sligo, F91 YW50, Ireland

HIGHLIGHTS

- Preparation of 2D metal-organic framework Cu₃(HHTP)₂ through hydrothermal.
- Cu₃(HHTP)₂ with modification of using carbon black (CB) and PEDOT: PSS.
- The MOF/CB/PEDOT: PSS exhibited a specific capacitance of 336.93 mF cm^{-2}
- The flexible electrochemical capacitor exhibited energy density 29.31 μW h cm^{-2}.

GRAPHICAL ABSTRACT
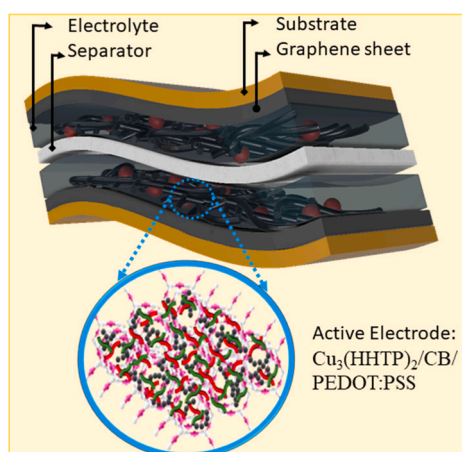
ARTICLE INFO

ABSTRACT

Hydrothermally synthesized 2D metal-organic framework (MOF) Cu₃(HHTP)₂ was modified with carbon black (CB) and poly(3,4-ethylenedioxythiophene)-poly(styrenesulfonate) (PEDOT: PSS) to develop a flexible energy storage device. The efficiency of electron transfer and ionic diffusion within the pristine MOF was enhanced in the composites of MOFs. The MOF/CB/PEDOT: PSS (20 %) composite demonstrated more than 110 times higher capacitance compared with pristine MOF-based devices, reaching 336.93 mF cm^{-2} (146.51 F g^{-1}) at 0.1 mA cm^{-2}. The developed device exhibited energy and power densities of 29.31 μW h cm^{-2} (12.86 Wh.kg^{-1}) and 39.38 μW cm^{-2} (17.28 W kg^{-1}), respectively. The addition of CB and PEDOT: PSS into the Cu₃(HHTP)₂ MOF decreased the pore structure due to the incorporation of solid materials in the pores and an excellent conductive channel for ion transfer. The study reveals that modifying the electrical, mechanical, and electrochemical properties of a 2D MOF can lead to the design of a high-performance flexible energy storage device for portable and wearable electronics.

---

* Corresponding author.
 E-mail address: L.Manjakkal@napier.ac.uk (L. Manjakkal).

1. Introduction

Metal-organic frameworks (MOFs) are considered one of the finest materials for flexible electrochemical device fabrication [1–3]. The physical arrangement of constituent components, including frameworks and porous structures, significantly influences several properties of MOFs, such as their specific surface area, transport routes, electrical conductivity, and structural stability [4,5]. Pristine MOFs' electrochemical performances mostly depend on their structural characteristics and chemical compositions [4]. However, the poor electrical conductivity, particle agglomeration (reducing porosity), and deterioration of electrode materials during long-time operation hinder the widespread use of MOFs in electrochemical devices [6,7]. Various conventional designs have been developed to increase MOFs' electrical conductivity and structural resilience at the micro/nanoscale level. These designs include one-dimensional (1D), two-dimensional (2D), and three-dimensional (3D) structures, which provide a favourable contribution to the total electrochemical performance [4,5]. Among these, 2D MOF offers unique physicochemical properties, tuneable chemical compositions, high active surface sites, and mechanical properties for developing flexible devices [8,9]. These parameters are crucial in determining their capacity to facilitate the movement of electrons and ions in energy storage devices. The large surface area and pore structure enhance ion adsorption and redox reaction for ion storage in the energy storage device [8,9]. Due to their unique characteristics, MOFs are promising for flexible electrochemical devices. Their variable porosity enables efficient ion and molecule transport, which is critical for battery and supercapacitor performance. Their possibility for miniaturisation enables the development of tiny devices. Table S1 shows the comparison of the various MOF-based energy storage devices. The low conductivity compared to other 2D materials including graphene, restricts its practical implementation of flexible energy storage devices [10]. These limitations can be minimized by using MOF composite and their derivatives.

In this work, we introduce a conductive 2D MOF-based composite electrode with carbon black (CB) and poly(3,4-ethylenedioxythiophene) polystyrene sulfonate (PEDOT: PSS) for the development of a flexible electrochemical capacitor (FEC) as an energy storage device. For this, a pristine 2D MOF, $Cu_3(HHTP)_2$, was prepared by facile hydrothermal synthesis. To enhance the electrochemical and ion-storing performances of the pristine MOF material, two additives were introduced, CB and PEDOT: PSS, into the structure. The primary challenge in enhancing the electrochemical performance of most MOFs has consistently been their low conductivity, which reduces electron transfer [11]. The CB, with high electrical conductivity and a large specific surface area, contributed to increasing the overall surface area of the electrode, thereby enhancing its charge storage capacity [12]. The PEDOT: PSS was incorporated to improve electrical conductivity and facilitate effective binding between the solid components and the graphene current collector used to fabricate the FEC. Here, the PEDOT: PSS enhances energy-storing performance due to pseudocapacitance and electrochemical double-layer (*edl*) formation [13]. Adding CB and PEDOT: PSS into the $Cu_3(HHTP)_2$ MOF was shown to lead to a decrease in the pore structure via the incorporation of solid materials in the pores and the creation of a new conductive channel for ion transfer. Consequently, these materials often exhibit desirable characteristics such as high electrical conductivity, favourable chemical stability, significant specific surface areas, and mechanically flexible properties [12]. These surface and bulk properties lead to substantial enhancement in energy storage such as the developed MOF/CB/PEDOT: PSS (20 %) based FEC showing a specific capacitance of 336.98 mF cm^{-2} at current density 100 μA cm^{-2}, which is more than 110 times higher compared to the prepared pristine MOF-based FEC, which exhibits 3 mF cm^{-2} at the same current density. This value is comparable with the reported performances of MOF-based energy storage devices and is summarized in Table S1 in supporting information.

2. Experimental section

Preparation of 2D $Cu_3(HHTP)_2$ MOF: To synthesize $Cu_3(HHTP)_2$, a solution of Copper (II) nitrate trihydrate and ammonia was prepared by weighing approximately 0.127 g $Cu(NO_3)_2 \cdot 3H_2O$ and 1.226 ml of 28 % aqueous ammonia in 2 mL of distilled water. The resulting royal blue solution was then added dropwise to a dispersion of HHTP (0.103 g) in 8.2 mL of distilled water. The reaction mixture was carefully placed in a preheated oven and maintained at 80 °C for 24 h. The mixture was allowed to cool to room temperature. The supernatant layer was discarded, and the rest of the mixture was washed with water (3 × 30 mL), ethanol (3 × 30 mL), and acetone (3 × 30 mL) in successive steps via centrifugation at 14,000 rpm to remove any impurities. Subsequently, the precipitate was filtered, yielding a dark blue powder (image is shown in Fig. S1 in the supporting information). The powder was dried at 80 °C for 72 h to obtain a dry and purified product. The resulting $Cu_3(HHTP)_2$ powder was then stored carefully for future use.

Electrodes and FEC Fabrication: The fabrication process of $Cu_3(HHTP)_2$ MOF-based electrodes for FEC applications was conducted as follows. Initially, a graphene sheet measuring 1 cm × 1 cm was carefully chosen as the current collector and evenly bonded onto a PVC substrate. The selection of graphene was based on its outstanding electrical conductivity and high surface area, which are critical attributes for efficient charge storage in ECs. The fabrication steps of the FECs are given in Fig. 1a. In this work, we prepared four different types of symmetric FEC, which consist of (i) MOF vs MOF (FEC1) (ii) MOF/CB vs MOF/CB (FEC2) (iii) MOF/CB/PEDOT: PSS (10 %) vs MOF/CB/PEDOT: PSS (10 %) (FEC3) and (iv) MOF/CB/PEDOT: PSS (20 %) MOF/CB/PEDOT: PSS (20 %) (FEC4). The schematics of the prepared electrode structure for the ion transfer for the individual FEC are given in Fig. 1b-d. For all electrodes, a wire was attached using Ag paste (RS components) for an external electrode connection and heated in an oven at 80 °C for 30 min. Symmetric FEC was developed with a cellulose/polyester cloth as a separator and a 6M LiCl solution as the electrolyte. Finally, the FECs were packed by using cling films. Schematic representations of the FEC4 (similar configuration for FEC3) are shown in Fig. 1e. Figs. S2a and S2b represent the FEC1 and FEC2 device structures. Here, for the preparation of the electrodes of FEC1, the active material for the electrodes was made from the MOF material. To prepare the $Cu_3(HHTP)_2$ MOF paste, the MOF material (100 wt%) was ground with a mixture of ethyl cellulose (40 wt%) and terpinol using a mortar and pestle. Ethyl cellulose was utilized as the binder, effectively holding the MOF particles together, while terpinol acted as the solvent, facilitating the formation of a homogenous paste. The well-dispersed $Cu_3(HHTP)_2$ MOF paste was then carefully hand-painted onto the surface of the graphene-based electrode, ensuring uniform coverage and strong adherence. After application, the assembled electrode underwent a drying process at 80 °C for approximately 30 min to eliminated residual solvent and established a stable and mechanically robust electrode structure. For the preparation of the electrodes of FEC2, the active material for the electrodes was prepared by taking MOF (90 wt%), carbon black (10 wt%), ethyl cellulose (40 wt%) and grinding them together with terpinol. The paste was hand-painted on the top of the graphene current collector and dried at 80 °C for half an hour. For the preparation of the electrodes of FEC3 and FEC4, the CB was fixed at 10 wt% and PEDOT: PSS (Oscilla) dissolved in dimethyl sulfoxide (DMSO) concentration varying in the range of 10 wt% (FEC3) to 20 wt% (FEC4). Similar to the preparation methods mentioned above, a paste was prepared using MOF, CB, and PEDOT: PSS and ethyl cellulose. The mixture was ground together using terpinol to form a fine paste then coated on the graphene electrodes and dried at 80 °C for half an hour in the oven.

Characterisation: Scanning electron microscopy (SEM), mainly used for particle morphology screening, was carried out with a TESCAN-VEGA 3 scanning electron microscope at a working distance of 15 mm and an accelerating voltage of 20 kV. The energy-dispersive X-ray (EDX) of the $Cu_3(HHTP)_2$ sample was also carried out using the same

experimental setup. The Fourier Transform Infrared Spectroscopy (FTIR) of the sample was obtained using a PerkinElmer spectrometer. Powder X-ray diffraction (XRD) patterns were measured in transmission using a STOE Stadi P diffractometer (Darmstadt, Germany) with CuKα1 radiation with a wavelength of $\lambda = 1.5406$ Å and a Ge (111) monochromator. The powders were ground before the measurement. Raman inVia spectrometer (Renishaw, Wotton-under-Edge, UK) was used for the Raman experiment. Raman excitation wavelength was 785 nm, 10 % lacer power and an X20 microscope objective was used. The electrochemical characterization determined the performance of the fabricated ECs. All electrochemical characterizations were done using Modulab™ software. The cyclic voltammetry (CV) (5–1000 mV s^{-1}), electrochemical impedance spectroscopy (EIS) (10 mHz to 1 MHz) and galvanostatic charge and discharge (GCD) experiments were performed to determine the specific capacitance, energy, and power density. The equation used to calculate specific capacitance, energy density, and power density is based on previously reported work [13].

3. Results and discussion

The pristine MOF-based electrode shows an evenly distributed pore structure with flake-like morphology as shown in Fig. 2a in the SEM image. These large pores are open channels that are sufficiently spacious to accommodate ions from the electrolyte and facilitate the ion's transportation. The SEM images of the electrodes fabricated with the addition of CB (Fig. 2b) and PEDOT: PSS (Fig. 2c and d) to Cu$_3$(HTTP)$_2$ were also taken. The SEM indicates that the additives have been incorporated within the pores of Cu$_3$(HTTP)$_2$-MOF. The SEM image of Cu$_3$(HHTP)$_2$/CB/PEDOT: PSS electrodes, given in Fig. 2d, shows that the porous nature gradually disappeared, indicating that the solid components have effectively been incorporated within the pores. The magnified images of the different electrodes are given in Figs. S3a–S3h in the supporting information. The pores distribution of the electrode was determined using ImageJ™ software and is discussed in Fig. S4.

The EDX analysis showed a clear and even distribution of the elements throughout the samples. The elemental mapping of Cu$_3$(HHTP)$_2$ MOF (given in Fig. S5) shows the presence of Copper (49.7 wt%), carbon (34.6 wt%), and oxygen (15.7 wt%), along with minor traces of sulphur and silicon. In distinct electrode configurations such as MOF/CB/ PEDOT: PSS (10 % and 20 %), EDX data indicates the presence of sulphur. The sulphur content rises from 0.2 wt% to 0.9 wt% as PEDOT: PSS concentration increases from 10 % to 20 %.

The FTIR identifies functional groups and chemical bonds inside the MOF and composite electrode. The coordination between metal ions and ligands was investigated by the FTIR spectrum, as given in Fig. 2e. Fig. 2e shows the comparative plot for all four printed electrodes. Different peaks correspond to the C-H, C-O, C=C and O-H stretching modes at 550–850, 1200–1350, 1450–1600 and 3000-3250 cm^{-1}. A low-frequency peak around 563 cm^{-1} in all MOFs is assigned to the metal–O (M − O) stretching vibrations. The lower region peaks are the result of the bond between the HHTP (benzene rings based) linker and metal ions (Cu) and the bond between water molecules attached with the HHTP linker and metal ions which is evidence of the formation of synthesized MOF. Besides, the strong characteristic peaks at about 1450 cm^{-1} in all MOF samples correspond to a metal–semiquinone stretch, an intermediate state between the metal–quinone and catecholate complexes. The spectrum of Cu$_3$(HHTP)$_2$ presented two strong peaks at 1214 and 1446 cm^{-1}, corresponding to C–O stretching vibration and C–H scissoring vibration, respectively. A broad absorption band at 3000–3400 cm^{-1} was observed, responsible for the hydrogen-bonded O–H stretching vibration [14].

The Cu$_3$(HHTP)$_2$ crystallinity of the sample was assessed via XRD, revealing distinct diffraction peaks at 2θ values of 5.01, 9.58, and 12.5, as given in Fig. 2f. These measurements indicate a well-defined long-range order within the square-planar plane [15]. The pronounced peaks at 2θ = 27.6 also signify long-range order along the axis, consistent with expectations for covalently linked layered materials. These 2θ values correspond to the crystal phases (100), (200), (210), and (002) respectively. All these peaks confirm the crystalline nature of the sample and are consistent with findings in previously reported literature [15–18]. The Raman spectra of electrodes are displayed in Fig. 2g. The Raman spectra from all four samples possessed major peaks at the G band and D band revealing the presence of sp^2 hybridised carbon and structural disorder [19]. Further, the Raman peak in the 120–160 cm^{-1} region is related to the metallic ions vibration [16]. The first-order G band (~1580 cm^{-1}), the doubly-resonant second order D band (1300–1400 cm^{-1}) [and 2D band (2600–2700 cm^{-1}) and the D' band (~1620 cm^{-1}) [20]. The structural characterisations strengthen our evidence for the
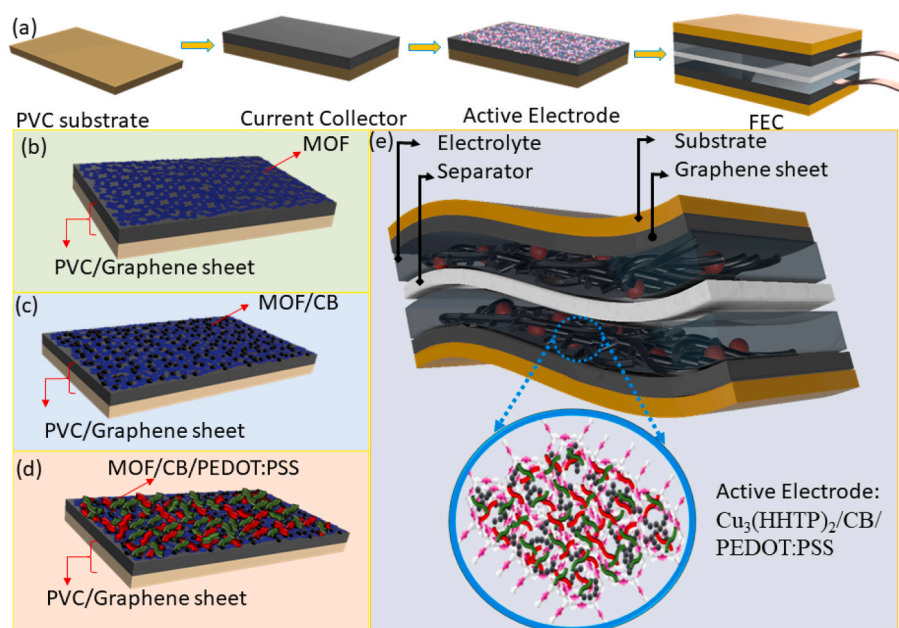

Fig. 1. (a) Electrodes and FEC fabrication steps. Schematics of the prepared various electrodes for (b) MOF (c) MOF/CB (d) MOF/CB/PEDOT: PSS-based films on a graphene sheet. (e) Schematic representation of the developed FEC4.
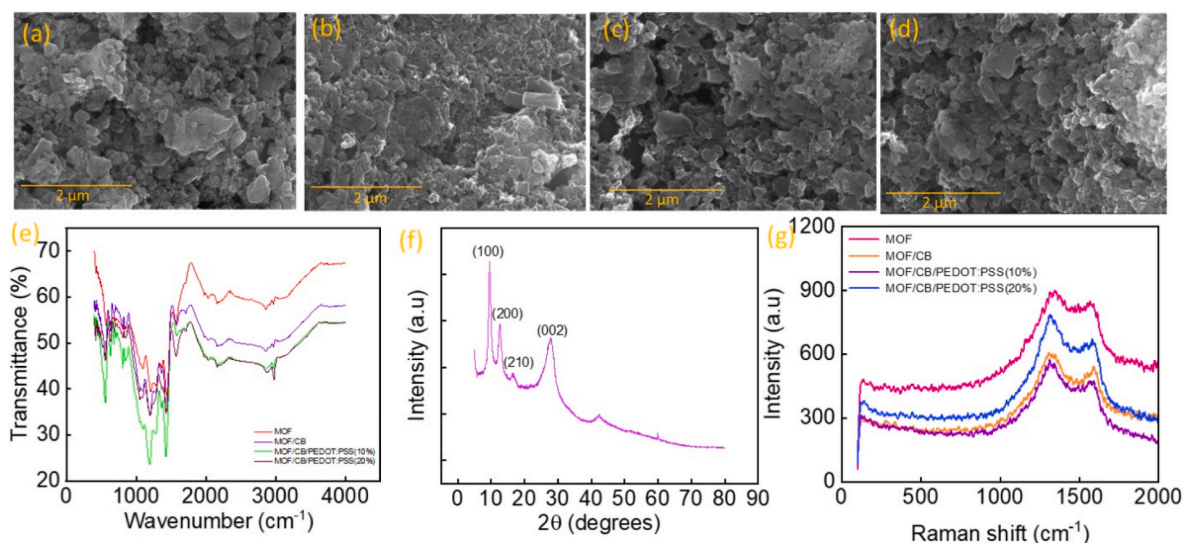
Fig. 2. (a)–(d) SEM images of MOF, MOF/CB. MOF/CB/PEDOT: PSS (10 %) and MOF/CB/PEDOT: PSS (20 %) electrodes, respectively. (e) FTIR spectrum of the MOF, MOF/CB. MOF/CB/PEDOT: PSS (10 %) and MOF/CB/PEDOT: PSS (20 %) films (f) XRD pattern of $Cu_3(HHTP)_2$ (g) Raman Spectra of the MOF, MOF/CB, MOF/CB/PEDOT: PSS (10 %) and MOF/CB/PEDOT: PSS (20 %) films.

successful formation of $Cu_3(HHTP)_2$ MOF [16].

The CV curve for $Cu_3(HHTP)_2$ MOF shows a redox peak at lower scan rates, as the potential changes slowly with time, giving more time for electrochemical reactions to occur. However, the peaks are insignificant at higher scan rates, as shown in Fig. 3a. This high scan rate shows the rate capability and reversibility of the synthesized material and is shown in Fig. 3a and S6a. The CV of MOF/CB for FEC2 shows a significant improvement in the peak current and shape as shown in Fig. 3b. The addition of CB changes the peaks in the curve, which could be due to the influence of electrochemical double layer capacitance (EDLC) formation in the electrode layer [21]. The addition of carbon black to the MOF enhances the formation of an *edl* and improves overall capacitance by increasing the conductivity, reducing resistance and ensuring efficient electron movement. Its large surface area offers more places for the

adsorption of electrolyte ions, which is essential for creating a strong double layer. Additionally, CB contributes to the development of a more porous electrode structure, which improves ion penetration and active material utilisation. A high scan rate quasi-rectangle shape was observed for the CV curve at 1000 mV s^{-1} in Fig. 3b and S6b. A sharp increase in the current was observed in the case of FEC3, indicating that the conductive polymer has significantly contributed to the performance of the devices, as shown in Fig. 3c. The CV curve for the different scan rates of 5–1000 mV s^{-1} is given in Fig. S6c. Maximum performance was obtained when the concentration of PEDOT: PSS was increased from 10 to 20 %, and remained unchanged without significant distortion, implying its remarkable rate performance and capacitive reversibility. This FEC had a different and wider operating window ranging from −0.2 to 0.8 V, meaning that the electrochemical reactions within the system span over
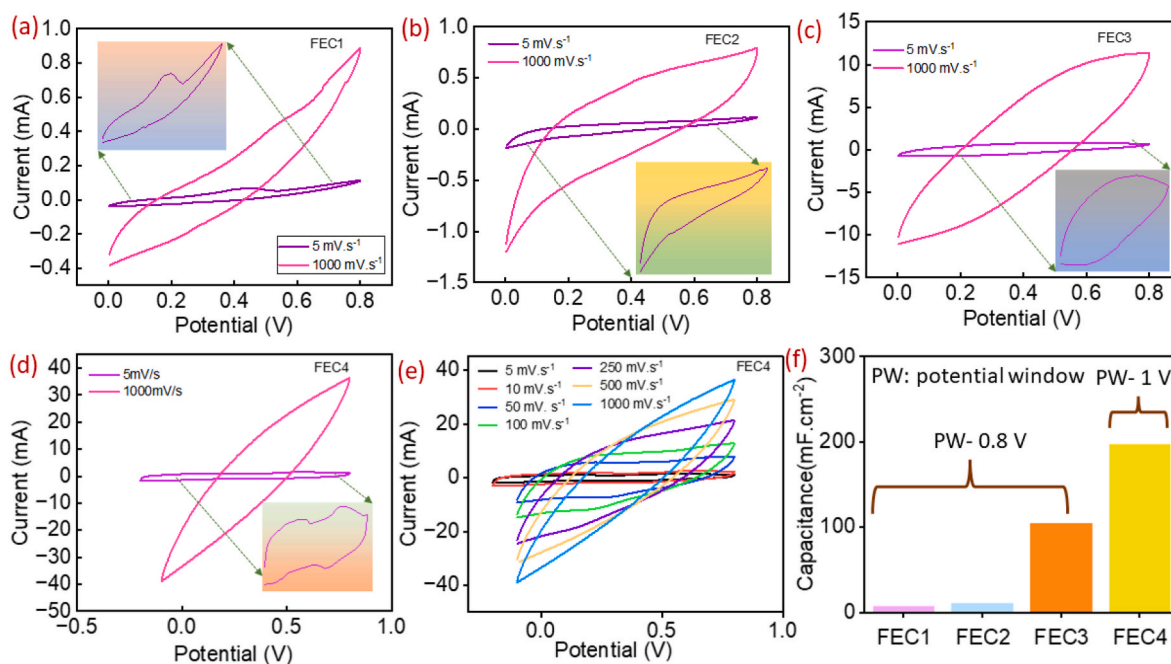

Fig. 3. (a)–(d) CV curve for low (5 mV s^{-1}) and high (1000 mV s^{-1}) scan rate for FEC1 -FEC4 respectively. (e) CV curve for FEC4 in the range of 5–1000 mV s^{-1}. (f) Specific capacitance of FEC1 to FEC4 at 5 mV s^{-1}.

a more significant potential, as shown in Fig. 3d. In lower scan rates, minor redox peaks were observed for the FEC4, which could be due to the high contribution of PEDOT: PSS into the composite. The redox peaks disappear for the high scan rate, as shown in Fig. 3e. Redox peaks in cyclic voltammetry become less noticeable at faster scan rates because the electrochemical reactions are unable to keep up with the rapid potential changes. During higher scan rates, the ions in the electrolyte do not have enough time to diffuse to the pores of the electrode, limiting the redox reaction. Also, the process capacitive current, which increases with the scan rate, dominates the redox peaks [22]. A comparison of the CV curve for all devices at 100 mV s^{-1} is given in Fig. S6d. The specific capacitance was measured from the absolute area of the CV curve, and it was observed that for FEC4 the value at 5 mV s^{-1} is 155.15 mF cm^{-2} and is much higher than for pristine MOF, which is 8.08 mF cm^{-2}. The variation of capacitance with scan rate for FEC1-FEC4 is given in Fig. S7.

The GCD plots of FEC1 to FEC4 are shown in Figs. S8a–S8c and Fig. 4a and exhibit a combined EDLC and pseudocapacitive behaviour for all devices. The GCD was measured for all devices for a potential window of 0.8 V. The value of specific capacitance (C_A), energy density (E_A) and power density (P_A) were measured from the GCD plots and are summarized in Tables S2a–S2d for all devices. The pristine MOF shows a significant voltage drop without surface and bulk properties modification using conductive fillers and conjugated conductive polymer. For example, 0.1 mA cm^{-2} for pristine MOF-based FEC shows a voltage drop of 0.3 V which is reduced with the addition of CB and is found to be 0.132 V. The voltage drop is significantly reduced with the addition of CB/PEDOT: PSS in the MOF and is measured at 0.005V for FEC4. The lack of conductivity and ion-storing ability leads to the high voltage drop and low performance of the MOF. For constant applied current density such as 0.1 mA cm^{-2}, the FEC 1 exhibits specific capacitance of 3 mF cm^{-2} and for MOF/CB (FEC2), the value increases to 8.704 mF cm^{-2}. Adding PEDOT: PSS significantly enhances the specific capacitance and is found to be 336.98 mF cm^{-2} (146.51 F g^{-1}) for FEC4. This also leads to improving the energy density of the device and for FEC4 at low current density such as 0.1 mA cm^{-2} the energy and power density are 29.31 μW h cm^{-2} (12.86 Wh.kg^{-1}) and 39.38 μW cm^{-2} (17.28 W kg^{-1}), respectively. The variation of energy-storing parameters is given in Tables S2a–S2d. The measurements reveal the excellent performance of composite devices such as FEC4. Fig. 4b shows the variation of specific capacitance energy and power density of FEC4 with various current densities. We also evaluated the long charge-discharging performance of the device over 5000 cycles with an operating potential of 0.8V. The MOF/CB/PEDOT: PSS (20 %) shows a capacitive retention of 75.63 % after 5000 cycles shown in Fig. S9a. The EIS test has been done at different points in between the cycles and it shows that the resistance of the material is increased slightly with the increase in cycles due to the degradation of the electrode and electrolyte which is given in Fig. S9b.

The efficiency of electron transfer and ionic diffusion inside the pristine composites of MOFs are verified with the charge transfer kinetics through the electrochemical impedance spectroscopic (EIS) analysis. The SEM analysis in Fig. 2a shows that the pristine MOF has large pores and open channels that are sufficiently spacious to accommodate electrolyte ions and facilitate the transportation of ions, schematically presented in Fig. 5a. This porous and conductive nature of the electrode leads to ionic diffusion. It can be found in the low-frequency region of the Nyquist plot shown in Fig. 5b. The straight line in the Nyquist plot towards the low-frequency region denotes the slow diffusion of ions from the electrolyte to the electrode. The unique structure and morphology of the synthesized Cu$_3$(HHTP)$_2$ MOF offers high-rate electrochemical performance [23]. The geometry of MOF provides direct paths for ions to diffuse and intercalate. For Cu$_3$(HHTP)$_2$ based devices such as FEC1, the equivalent series resistance (ESR) value which depicts the total intrinsic, contact and ionic resistance is found to be 6.41 Ω.cm^{-2}. The addition of CB into the layered and pore structure of Cu$_3$(HHTP)$_2$ as represented in Fig. 5c significantly decreases the ionic resistance and could be found from the Nyquist plot in Fig. 5d. Here the MOF is embedded into the CB composite and the pores are filled with conductive filler, as shown in the SEM image of Fig. 2b leading to enhanced specific surface area. Bulk conductivity modification for the favourable ion accessibility to the electrodes is indicated by the low impedance value (the imaginary impedance component) compared to pristine MOF as shown in Fig. S10. This further enables the decrease of the ESR value found to be 5.92 Ω. cm^{-2}. The addition of conjugated polymer PEDOT: PSS in the MOF/CB composite shows a drastic reduction in the impedance value. The MOF/CB with PEDOT: PSS component facilitates faster ion diffusion due to the low conductivity of the composite and is schematically given in Fig. 5e. This could be observed in the low-frequency range of the Nyquist plot for the MOF/CB with the 10 % and 20 % PEDOT: PSS combination. The high conductivity of the composite gives a very low ESR value of 1.61 Ω.cm^{-2} for FEC3 and 1.8 Ω. cm^{-2} for FEC4. Hence the combined CB and PEDOT: PSS leads to a drastic reduction in the ESR value, and the capacitive impedance as represented in Fig. 5f. In all devices, the lack of a semicircle at higher frequencies represents reduced charge transfer resistance (R$_{CT}$) and negligible values can be attributed to the highly conductive conjugated Cu$_3$(HHTP)$_2$ structure and the composite electrodes.

The decrease of the total impedance and the capacitive nature of the fabricated electrodes could be observed from the Bode impedance plot in Fig. S11 in supporting information. The Bode impedance decreases from 10 mHz to 100 kHz due to negligible charge transfer resistance and low ESR values. This is also confirmed by the Bode phase angle plot in Fig. 5g where the phase angle is negative. In the low-frequency region, such as 10 mHz, the phase angle has values of −19.90 $^\circ$, −25.02 $^\circ$, −52.17° and -68.55° corresponding to FEC1 and FEC4, as illustrated in Fig. 5h. These values show the capacitive nature of the electrodes with capacitance measured and plotted in Fig. 5i. Compared with pristine MOF, the MOF with CB and PEDOT: PSS (20 %) shows more than 13 times higher capacitance value. This high capacitance could be due to the
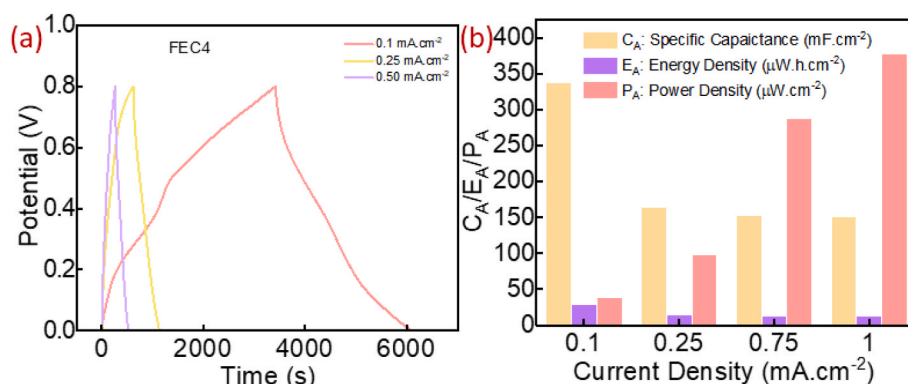

Fig. 4. (a) GCD plots for FEC4 (b) The performances of FEC4, specific capacitance, energy, and power density with various current densities.
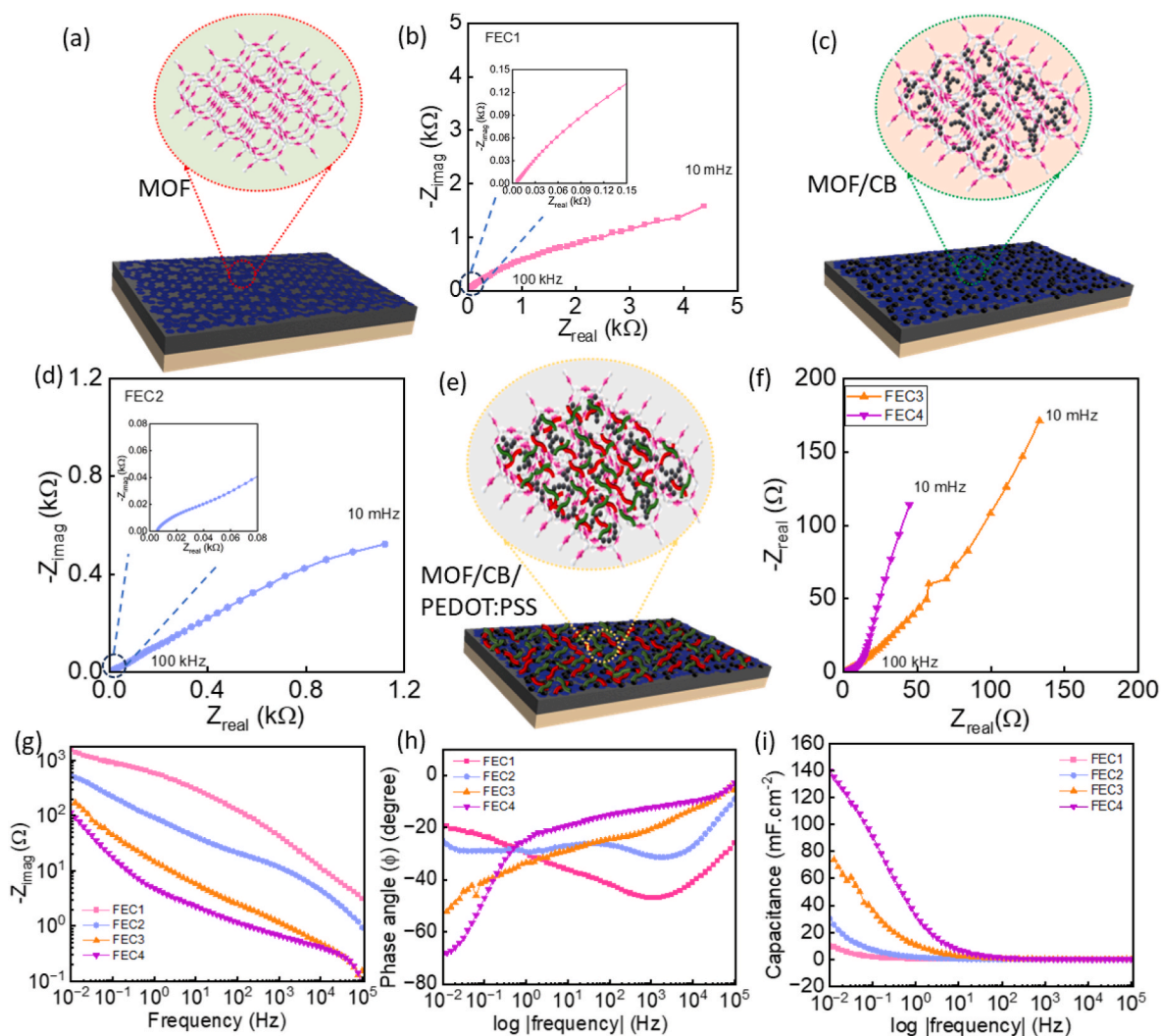
Fig. 5. (a) Schematic illustration of the FEC1- Cu$_3$(HHTP)$_2$ electrode for ion transport (b) Nyquist plot of FEC1 (c) Schematic illustration of the FEC2- Cu$_3$(HHTP)$_2$/CB electrode for ion transport (d) Nyquist plot of FEC2 (e) Schematic illustration of the FEC3 and FEC4 - Cu$_3$(HHTP)$_2$/CB/PEDOT: PSS electrode for ion transport (f) Nyquist plot of FEC3 and FEC4 (g) Variation of imaginary impedance component with frequency for FEC1-FEC4 (h) Bode phase angle plot for the FEC1 to FEC4 and (i) Variation of capacitance with frequency for FEC1-FEC4.
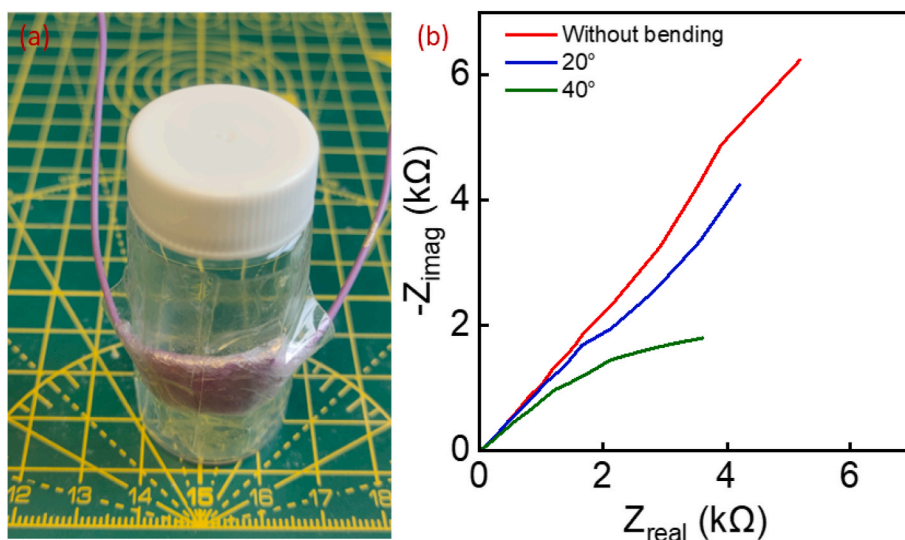

Fig. 6. (a) Image of FEC4 which shows the flexibility of the device. (b) Nyquist plot for FEC in different bending angles.

contribution from CB and PEDOT: PSS and its interaction with MOF.

To evaluate the FEC's bendability, the device is bent to various degrees between 20^0 and 40^0. Fig. 6a depicts the flexibility of FEC4 at various degrees of bending. EIS analysis is performed at various bending angles to evaluate the variation of electrical properties under the bending angle. The FEC shows a decrease in the ionic resistance in low frequency during bending as shown in the EIS analysis from 10 mHz to 1 MHz as shown in Fig. 6b. The change in resistance is due to the variation in the electrode/electrolyte interaction under bending. Similarly, the CV analysis was also done at different bending degrees (20^0 and 40^0) and this can be shown in the supporting information Fig. S12 and it shows the variation of area under the CV curve with bending angle. During bending, the electrode gets compressed, and reducing the gap between the electrode and electrolyte enhances the wetting of the electrode, which provides better ion access to the active sites [24]. Additionally, this compression may restructure the internal pore structure, spreading the electrolyte more uniformly throughout the electrode and establishing more direct ion pathways. At the microscopic level, bending improves interfacial bonding and reduces resistance at the reaction sites by strengthening the contact between the electrode and electrolyte.

4. Conclusions

This study demonstrates the development of high-performance flexible electrochemical energy storage devices using $Cu_3(HHTP)_2$ 2D metal-organic frameworks (MOFs) as electrodes. By modifying the pristine MOF with carbon black (CB) and poly(3,4-ethylenedioxythiophene)-poly (styrenesulfonate) (PEDOT: PSS), we significantly enhanced the electron transfer and ionic diffusion within the composite materials. The addition of CB and PEDOT: PSS led to a substantial increase in capacitance, with the MOF/CB/PEDOT: PSS (20 %) composite exhibiting more than 110 times higher capacitance compared to pristine MOF-based devices. The FEC fabricated based on MOF/CB/PEDOT: PSS (20 %) showed a specific capacitance of 336.98 mF cm^{-2}, with energy and power density are 29.31 μW h cm^{-2} and 39.38 μW cm^{-2}, respectively, at low current density such as 0.1 mA cm^{-2}. We analyzed this aspect by bending the device at various angles from 20 to 40°, observing an increase in capacitance. This increase can be attributed to the reduced distance between electrodes and the corresponding decrease in resistance.

CRediT authorship contribution statement

Maria Prince: Writing – original draft, Methodology, Investigation, Formal analysis, Data curation. **Jithin Kanathedath:** Writing – original draft, Visualization, Methodology, Investigation. **Febin Paul:** Writing – original draft, Methodology, Investigation, Formal analysis. **Prasutha Rani Markapudi:** Investigation, Formal analysis, Data curation. **Mustehsan Beg:** Methodology, Investigation, Formal analysis. **Lynn Paterson:** Writing – original draft, Methodology, Investigation, Formal analysis. **Marc PY. Desmulliez:** Writing – review & editing, Investigation, Formal analysis, Data curation. **Suresh C. Pillai:** Writing – original draft, Funding acquisition, Formal analysis, Data curation. **Libu Manjakkal:** Writing – review & editing, Writing – original draft, Visualization, Validation, Supervision, Resources, Project administration, Methodology, Investigation, Funding acquisition, Formal analysis, Data curation, Conceptualization.

Declaration of competing interest

The authors declare that they have no known competing financial interests or personal relationships that could have appeared to influence the work reported in this paper.

Appendix A. Supplementary data

Supplementary data to this article can be found online at https://doi.org/10.1016/j.jpowsour.2025.236214.

Data availability

Data will be made available on request.

References

[1] C. Li, Q. Zhang, J. Sun, T. Li, S. E, Z. Zhu, B. He, Z. Zhou, Q. Li, Y. Yao, High-performance quasi-solid-state flexible aqueous rechargeable Ag–Zn battery based on metal–organic framework-derived Ag nanowires, ACS Energy Lett. 3 (11) (2018) 2761–2768.

[2] T. Qiu, Z. Liang, W. Guo, H. Tabassum, S. Gao, R. Zou, Metal–organic framework-based materials for energy conversion and storage, ACS Energy Lett. 5 (2) (2020) 520–532.

[3] J. Liu, X.Y.D. Ma, Z. Wang, L. Xu, F. Wang, C. He, X. Lu, Metal–organic framework-based flexible devices with simultaneous electrochromic and electrofluorochromic functions, ACS Appl. Electron. Mater. 3 (3) (2021) 1489–1495.

[4] D. Tian, C. Wang, X. Lu, Metal–organic frameworks and their derived functional materials for supercapacitor electrode application, adva, Energy Sustain. Res. 2 (7) (2021) 2100024.

[5] N. Kitchamsetti, J.S. Cho, A roadmap of recent advances in MXene@MOF hybrids, its derived composites: synthesis, properties, and their utilization as an electrode for supercapacitors, rechargeable batteries and electrocatalysis, J. Energy Storage 80 (2024) 110293.

[6] Y. Xu, Q. Li, X. Guo, S. Zhang, W. Li, H. Pang, Metal organic frameworks and their composites for supercapacitor application, J. Energy Storage 56 (2022) 105819.

[7] R. Du, Y. Wu, Y. Yang, T. Zhai, T. Zhou, Q. Shang, L. Zhu, C. Shang, Z. Guo, Porosity engineering of MOF-based materials for electrochemical energy storage, Adv. Energy Mater. 11 (20) (2021) 2100154.

[8] J. Liu, X. Song, T. Zhang, S. Liu, H. Wen, L. Chen, 2D conductive metal–organic frameworks: an emerging platform for electrochemical energy storage, Angew. Chem. 133 (11) (2021) 5672–5684.

[9] K.W. Nam, S.S. Park, R. dos Reis, V.P. Dravid, H. Kim, C.A. Mirkin, J.F. Stoddart, Conductive 2D metal-organic framework for high-performance cathodes in aqueous rechargeable zinc batteries, Nat. Commun. 10 (1) (2019) 4948.

[10] D. Xiong, X. Deng, Z. Cao, S. Tao, Z. Song, X. Xiao, W. Deng, H. Hou, G. Zou, X. Ji, 2D metal–organic frameworks for electrochemical energy storage, Energy Environ. Mater. 6 (6) (2023) e12521.

[11] S. Huang, X.-R. Shi, C. Sun, Z. Xhang, M. Huang, R. Liu, H. Wang, S. Xu, Template-controlled in-situ growing of NiCo-MOF nanosheets on Ni foam with mixed linkers for high performance asymmetric supercapacitors, Appl. Surf. Sci. 572 (2022) 151344.

[12] M. Beg, K.M. Alcock, A. Titus Mavelil, D. O'Rourke, D. Sun, K. Goh, L. Manjakkal, H. Yu, Paper supercapacitor developed using a manganese dioxide/carbon black composite and a water hyacinth cellulose nanofiber-based bilayer separator, ACS Appl. Mater. Interfaces 15 (44) (2023) 51100–51109.

[13] L. Manjakkal, A. Pullanchiyodan, N. Yogeswaran, E.S. Hosseini, R. Dahiya, A wearable supercapacitor based on conductive PEDOT:PSS-coated cloth and a sweat electrolyte, Adv. Mater. 32 (24) (2020) 1907254.

[14] K. Niu, P. Sun, J. Chen, X. Lu, Dense conductive metal–organic frameworks as robust electrocatalysts for biosensing, Anal. Chem. 94 (49) (2022) 17177–17185.

[15] M. de Lourdes Gonzalez-Juarez, C. Morales, J.I. Flege, E. Flores, M. Martin-Gonzalez, I. Nandhakumar, D. Bradshaw, Tunable carrier type of a semiconducting 2D metal–organic framework Cu3(HHTP)2, ACS Appl. Mater. Interfaces 14 (10) (2022) 12404–12411.

[16] M.Z. Iqbal, M. Shaheen, M.W. Khan, S. Siddique, S. Farid, S. Aftab, S.M. Wabaidur, The rise of 2D conductive metal-organic framework: Cu3(HHTP)2 d-π MOF for integrated battery-supercapacitor hybrids, Mater. Today Sustainability 22 (2023) 100331.

[17] F. Wu, W. Fang, X. Yang, J. Xu, J. Xia, Z. Wang, Two-dimensional π-conjugated metal-organic framework with high electrical conductivity for electrochemical sensing, J. Chin. Chem. Soc. (Taipei, Taiwan) 66 (5) (2019) 522–528.

[18] W. Zhao, T. Chen, W. Wang, S. Bi, M. Jiang, K.Y. Zhang, S. Liu, W. Huang, Q. Zhao, Layer-by-Layer 2D ultrathin conductive Cu3(HHTP)2 film for high-performance flexible transparent supercapacitors, Adv. Mater. Interfac. 8 (11) (2021).

[19] H. Lim, H. Kwon, H. Kang, J.E. Jang, H.-J. Kwon, Semiconducting MOFs on ultraviolet laser-induced graphene with a hierarchical pore architecture for NO2 monitoring, Nat. Commun. 14 (1) (2023) 3114.

[20] Z. Li, L. Deng, I.A. Kinloch, R.J. Young, Raman spectroscopy of carbon materials and their composites: graphene, nanotubes and fibres, Prog. Mater. Sci. 135 (2023) 101089.

[21] J.S. Stefano, L.R.G.e. Silva, B.C. Janegitz, New carbon black-based conductive filaments for the additive manufacture of improved electrochemical sensors by fused deposition modeling, Microchim. Acta 189 (11) (2022) 414.

[22] X. Pu, D. Zhao, Ch Fu, Z. Chen, S. Cao, C. Wang, Y. Cao, Understanding and calibration of charge storage mechanism in cyclic voltammetry curves, Angewandte Chem. Int. 60 (2021) 21310–21318.

[23] K.M. Snook, L.B. Zasada, D. Chehada, D.J. Xiao, Oxidative control over the morphology of Cu3 (HHTP)2, a 2D conductive metal–organic framework, Chem. Sci. 13 (35) (2022) 10472–10478.

[24] J. Xu, J. Lei, N. Ming, C. Zhang, K. Huo, Rational design of wood-structured thick electrode for electrochemical energy storage, Adv. Funct. Mater. 32 (2022) 2204426.